View Online / Journal Homepage / Table of Contents for this issue
Dynamic Article Links

Dalton Transactions

Cite this: *Dalton Trans.*, 2012, **41**, 5343

www.rsc.org/dalton

PAPER

Efficient energy transfer *via* the cyanide bridge in dinuclear complexes containing Ru(II) polypyridine moieties†

Alejandro Cadranel,[a] Pablo Alborés,[a] Shiori Yamazaki,[b] Valeria D. Kleiman[b] and Luis M. Baraldo*[a]

Received 4th October 2011, Accepted 18th February 2012
DOI: 10.1039/c2dt11869f

Published on 26 March 2012 on http://pubs.rsc.org | doi:10.1039/C2DT11869F
Downloaded by University of Michigan Library on 26 April 2012

We report the synthesis, structure and properties of the cyanide-bridged dinuclear complex ions $[Ru(L)(bpy)(\mu\text{-}NC)M(CN)_5]^{2-/-}$ (L = tpy, 2,2′;6′,2″-terpyridine, or tpm, *tris*(1-pyrazolyl)methane, bpy = 2,2′-bipyridine, M = Fe(II), Fe(III), Cr(III)) and the related monomers $[Ru(L)(bpy)X]^{2+}$ (X = CN^- and NCS^-). All the monomeric compounds are weak MLCT emitters (λ = 650–715 nm, $\phi \approx 10^{-4}$). In the Fe(II) and Cr(III) dinuclear systems, the cyanide bridge promotes efficient energy transfer between the Ru-centered MLCT state and a Fe(II)- or Cr(III)-centered d–d state, which results either in a complete quenching of luminescence or in a narrow red emission ($\lambda \approx 820$ nm, $\phi \approx 10^{-3}$) respectively. In the case of Fe(III) dinuclear systems, an electron transfer quenching process is also likely to occur.

Introduction

In any system designed to interact with light, a crucial property is its ability to capture photons. One way to improve this characteristic is to create an ordered array of interactive chromophores where the energy can be channelled, mimicking the characteristics of biological light-harvesting antenna systems. Control over the energy and electron transfer can be achieved through manipulation of the nature, geometry, or distance between components of the array. Functional systems are difficult to achieve, not only due to their difficult synthesis, but also because the interaction between the molecular components can open reaction pathways where the energy is dissipated to useless heat.

Cyanide bridged complexes are good candidates for this type of array, and the exploration of their chemistry has revealed clusters of different nuclearities and geometries, and large systems like nanoparticles[1] and surfaces.[2] The choice of cyanide anion as a bridge is attractive for its ability to promote strong coupling between metallic fragments, and because it does not present acceptor states that may act as electron traps. Early work from the group of Scandola has shown that moieties linked by cyanide groups have the ability to undergo energy transfer between them.[3]

Table 1 Complexes reported in this work

L	X	Compound
tpy	CN^-	**1a**
	NCS^-	**2a**
	$(\mu\text{-}NC)Fe^{III}(CN)_5$	**3a**
	$(\mu\text{-}NC)Fe^{II}(CN)_5$	**3a^{red}**
	$(\mu\text{-}NC)Cr^{III}(CN)_5$	**4a**
tpm	CN^-	**1b**
	NCS^-	**2b**
	$(\mu\text{-}NC)Fe^{III}(CN)_5$	**3b**
	$(\mu\text{-}NC)Fe^{II}(CN)_5$	**3b^{red}**
	$(\mu\text{-}NC)Cr^{III}(CN)_5$	**4b**

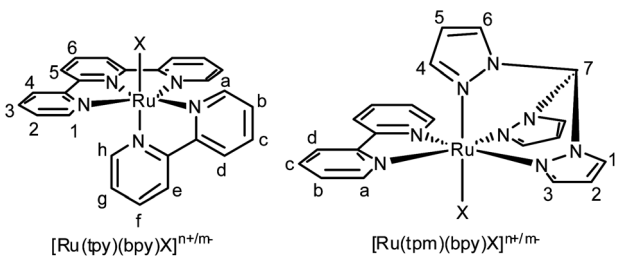

Scheme 1 Sketches of the complexes reported in this work, labeled to identify the different H atoms in ^{1}H NMR. Net charge differs from mononuclear to dinuclear species.

In this work, we report the synthesis, structure and properties of a family of dinuclear compounds combining a [Ru(L)(bpy)] (with L = tpy or tpm) chromophore and chromium or iron hexacyanometallates (Table 1). We also report the properties of corresponding mononuclear complexes [Ru(L)(bpy)(X)] (X = CN^- and NCS^-) for comparison purposes (see Scheme 1). Our aim is to identify dinuclear systems where the presence of an additional metal ion does not result in thermal deactivation of their excited

[a]*Departamento de Química Inorgánica, Analítica y Química Física, INQUIMAE, Facultad de Ciencias Exactas y Naturales, Universidad de Buenos Aires, Pabellón 2, Ciudad Universitaria, C1428EHA, Buenos Aires, Argentina. E-mail: baraldo@qi.fcen.uba.ar; Fax: +54-11-4576-3341; Tel: +54-11-4576-3380 int 127*
[b]*Department of Chemistry, University of Florida, Gainesville, FL 32611-7200, USA. E-mail: kleiman@chem.ufl.edu; Tel: +01-352-392-4656*

† Electronic supplementary information (ESI) available: CCDC reference numbers 843186–843192. For ESI and crystallographic data in CIF or other electronic format see DOI: 10.1039/c2dt11869f

states. Fragments with this property are good candidates for the design of systems of higher nuclearity that may act as efficient antennas for different applications.

Experimental

Materials

Tris(1-pyrazolyl)methane,[4] $[Ru(tpm)Cl_3]$,[5] $[Ru(tpm)(bpy)Cl]Cl$,[5] $[Ru(tpy)Cl_3]$[6] and $[Ru(tpy)(bpy)Cl]Cl$[7] were prepared according to previous reports. $(TPP)_3[Cr(CN)_6]$[8] and $(TPP)_3[Fe(CN)_6]$[9] (TPP = tetraphenylphosphonium) were synthesized using a slight variation of literature methods. Solvents for UV-visible and electrochemistry measurements were dried according to literature procedures.[10] The *N*-tetrabutylammonium hexafluorophosphate ($TBAPF_6$) used in the cyclic voltammetry experiments was recrystallized from ethanol. All other reagents were obtained commercially and used without further purification. All the compounds synthesized in this work were dried in a vacuum dessicator for at least 12 hours prior to characterization.

Synthesis of the complexes

[Ru(L)(bpy)CN](PF$_6$) (L = tpy (1a) or tpm (1b)). These synthesis are a variation of those described in ref. 11 and 12. In a typical preparation, 0.35 mmol of [Ru(L)(bpy)Cl]Cl (L = tpy, 197 mg; L = tpm, 202 mg) together with 10 eq. of KCN (230 mg) were dissolved in basic water (containing 0.2 g of NaOH in 50 mL of solution, in order to prevent HCN vapors). The mixture was heated to reflux for 2 hours, and 1.2 eq. of KPF_6 (L = tpy, 79 mg; L = tpm, 72 mg) were added to the hot solution. After cooling for 2 hours in the refrigerator, a solid appeared. The product was collected on a frit and washed with water (2 × 3 mL). Purification was achieved by recrystallization from acetonitrile. L = tpy: Yield: 120 mg of a violet crystalline solid (63.0%). Anal. Calcd for **1a·1.5H$_2$O**: C, 45.4; H, 3.2; N, 12.2. Found: C, 45.4; H, 3.2; N, 12.1. ^{1}H NMR (CD_3CN, 500 MHz), δ (ppm): 10.080 (ddd, 1H, J = 5.5 Hz, 1.5 Hz, 0.75 Hz, Ha), 8.569 (ddd, 1H, J = 8.5 Hz, 1.75 Hz, 0.75 Hz, Hd), 8.479 (d, 2H, J = 8.5 Hz, H5), 8.367 (ddd, 2H, J = 8 Hz, 1.5 Hz, 0.75 Hz, H4), 8.360 (ddd, 1H, J = 8.25 Hz, 1 Hz, 0.75 Hz, He), 8.217 (ddd, 1H, J = 8.5 Hz, 7.75 Hz, 1.5 Hz, Hc), 8.161 (t, 1H, J = 8.5 Hz, H6), 7.926 (ddd, 2H, J = 8 Hz, 7.5 Hz, 1.5 Hz, H3), 7.894 (ddd, 1H, J = 7.75 Hz, 5.5 Hz, 1.75 Hz, Hb), 7.816 (ddd, 1H, J = 8.25 Hz, 7.5 Hz, 1.5 Hz, Hf), 7.706 (ddd, 2H, J = 5.5 Hz, 1.5 Hz, 0.75 Hz, H1), 7.285 (ddd, 2H, J = 7.5 Hz, 5.5 Hz, 1.5 Hz, H2), 7.243 (ddd, 1H, J = 5.5 Hz, 1.5 Hz, 0.75 Hz, Hh), 7.091 (ddd, 1H, J = 7.5 Hz, 5.5 Hz, 1 Hz, Hg). L = tpm: Yield: 173 mg of a red solid (73.9%). Anal. Calcd for **1b·2H$_2$O**: C, 37.2; H, 3.3; N, 18.6. Found: C, 37.3; H, 3.0; N, 18.3. ^{1}H NMR (CD_3CN, 500 MHz) δ (ppm): 8.894 (s, 1H, H7), 8.645 (ddd, 2H, J = 5.75 Hz, 1.5 Hz, 0.5 Hz, Ha), 8.450 (ddd, 2H, J = 8 Hz, 1.25 Hz, 0.5 Hz, Hd), 8.348 (dd, 2H, J = 2.5 Hz, 1 Hz, H1), 8.285 (3H, m, H3 + H4), 8.052 (ddd, 2H, J = 8 Hz, 7.5 Hz, 1.5 Hz, Hc), 7.474 (ddd, 2H, J = 7.5 Hz, 5.75 Hz, 1.25 Hz, Hb), 6.703 (ddd, 1H, J = 2.25 Hz, 0.5 Hz, 0.5 Hz, H6), 6.647 (dd, 2H, J = 3 Hz, 2.5 Hz, H2), 6.302 (dd, 1H, J = 3 Hz, 2.25 Hz, H5).

[Ru(L)(bpy)(NCS)](SCN) (L = tpy (2a) or tpm (2b)). Proceeding in a similar way, 0.085 mmol of [Ru(L)(bpy)Cl]Cl (L = tpy 48 mg; L = tpm 46 mg) and 10 equivalents of KSCN (87 mg) were dissolved in 30 mL of water and heated to reflux for 2 hours. **2b** precipitated as an orange solid when the solution was cooled down to room temperature, whereas **2a** was reduced to 5–8 mL and formed a violet solid. After filtering and washing with water at room temperature (2 × 1 mL), the products were recrystallized from acetonitrile or acetonitrile–water. L = tpy: Yield: 20 mg (38.0%). Anal. Calcd for **2a·0.5H$_2$O**: C, 52.7; H, 3.3; N, 16.0; S, 10.4. Found: C, 52.7; H, 2.9; N, 15.5; S, 10.3. ^{1}H NMR (CD_3CN, 500 MHz), δ (ppm): 9.662 (ddd, 1H, J = 5.5 Hz, 1.5 Hz, 1 Hz, Ha), 8.602 (ddd, 1H, J = 8.5 Hz, 1.25 Hz, 1 Hz, Hd), 8.527 (d, 2H, J = 8 Hz, H5), 8.405 (ddd, 2H, J = 8 Hz, 1 Hz, 0.75 Hz, H4), 8.317 (ddd, 1H, J = 8Hz, 1.25 Hz, 0.75 Hz, He), 8.286 (ddd, 1H, J = 8.5 Hz, 8 Hz, 1.5 Hz, Hc), 8.202 (t, 1H, J = 8 Hz, H6), 8.008 (ddd, 1H, J = 8 Hz, 5.5 Hz, 1.25 Hz, Hb), 7.956 (ddd, 2H, J = 8Hz, 7.5 Hz, 1.5 Hz, H3), 7.721 (ddd, 1H, J = 8 Hz, 7.5 Hz, 1.5 Hz, Hf), 7.676 (ddd, 2H, J = 5.5 Hz, 1.5 Hz, 0.75 Hz, H1), 7.315 (ddd, 2H, J = 7.5 Hz, 5.5 Hz, 1 Hz, H2), 7.252 (ddd, 1H, J = 5.5 Hz, 1.5 Hz, 0.75 Hz, Hh), 6.993 (ddd, 1H, J = 7.5 Hz, 5.5 Hz, 1.25 Hz, Hg). L = tpm: Yield: 15 mg (30.6%). Anal. Calcd for **2b**: C, 45.0; H, 3.1; N, 23.8; S, 10.9. Found: C, 45.2; H, 3.0; N, 23.6; S, 10.8. ^{1}H NMR (CD_3CN, 500 MHz) δ (ppm): 9.125 (s, 1H, H7), 8.655 (ddd, 2H, J = 6Hz, 1.5 Hz, 1 Hz, Ha), 8.522 (ddd, 2H, J = 8.25 Hz, 1.25 Hz, 1 Hz, Hd), 8.451 (dd, 2H, J = 3 Hz, 0.5 Hz, H1), 8.333 (1H,dd, J = 3 Hz, 0.75 Hz, H4), 8.226 (2H,d, J = 2 Hz, H3), 8.103 (ddd, 2H, J = 8.25 Hz, 7.5 Hz, 1.5 Hz, Hc), 7.523 (ddd, 2H, J = 7.5 Hz, 6 Hz, 1.25 Hz, Hb), 6.712 (dd, 2H, J = 3 Hz, 2 Hz, H2), 6.602 (d, 1H, J = 2.25 Hz, H6), 6.259 (dd, 1H, J = 3 Hz, 2.25 Hz, H5). Hexafluorophosphate salts were obtained when needed by dissolving SCN^- salts together with 1.2 eq. of NH_4PF_6 in ACN, adding water and filtering the formed solid.

(TPP)[(L)(bpy)Ru(μ-NC)Fe(CN)$_5$] (L = tpy (3a) or tpm (3b)). 0.18 mmol of [Ru(L)(bpy)Cl]Cl (L = tpy, 101 mg; L = tpm, 104 mg) and 5 eq. of $(TPP)_3[Fe(CN)_6]$ (1.1 g) were dissolved in 60 mL of methanol and refluxed for 2 h. The hot solution was filtered and its volume reduced to ~5 mL. Purification by several exclusion chromatographies using a Sephadex LH-20 column (l = 60 cm, ϕ = 4 cm) packed and eluted with methanol was needed in order to remove the Fe monomer excess. The first, red- (L = tpy) or green-colored (L = tpm) fraction collected was rotavaporated to 5 mL, and 50 mL of water was added. One week later, rhomboid-shaped violet (tpy) or red (tpm) crystals were collected on a frit, washed with water (3 × 3 mL) and dried in the desiccator. L = tpy: Yield: 139 mg (69.3%). Anal. Calcd for **3a·4H$_2$O**: C, 59.3; H, 4.3; N, 13.8. Found: C, 59.2; H, 4.2; N, 13.9. L = tpm: Yield: 88 mg (43.2%). Anal. Calcd for **3b·6H$_2$O**: C, 53.1; H, 4.5; N, 17.3. Found: C, 53.3; H, 4.7; N, 17.3.

K$_2$[(L)(bpy)Ru(μ-NC)Fe(CN)$_5$] (L = tpy (3a^{red}) or tpm (3b^{red})). 100 mL of water were deoxygenated by bubbling argon for 30 min. Then, 0.18 mmol of [Ru(L)(bpy)Cl]Cl (L = tpy, 101 mg; L = tpm, 104 mg) and 6 eq. of $K_4[Fe(CN)_6]\cdot 3H_2O$ (456 mg) were dissolved, and the mixture heated at reflux for 4 hours under Ar atmosphere. The solvent was removed by

Published on 26 March 2012 on http://pubs.rsc.org | doi:10.1039/C2DT11869F
Downloaded by University of Michigan Library on 26 April 2012

This journal is © The Royal Society of Chemistry 2012

Published on 26 March 2012 on http://pubs.rsc.org | doi:10.1039/C2DT11869F
Downloaded by University of Michigan Library on 26 April 2012

distillation at low pressure with a N_2(l) trap until 40 mL remained. 300 mL of deoxygenated methanol were added and a solid was found to precipitate. It was removed by a Schlenk filter, and the solvent was evaporated by the technique described previously. The resulting red solid was dried in the desiccator. L = tpy: Yield: 96 mg (50.7%). Anal. Calcd for **3a^{red}·15H$_2$O**: C, 35.4; H, 4.7; N, 14.7. Found: C, 36.3; H, 3.5; N, 13.8. ^{1}H NMR (D_2O, 500 MHz) δ (ppm): 10.651 (d, 1H, Ha), 8.854 (d, 1H, Hd), 8.372 (d, 1H, He), 8.311 (t, 1H, Hc), 8.143 (t, 1H, Hb), 8.020 (d, 2H, H5), 7.954 (d, 2H, H4), 7.750 (d, 2H, H1), 7.577 (t, 2H, H3), 7.515 (m, 2H, Hf + H6), 7.177 (t, 2H, H2), 7.013 (t, 1H, Hg), 6.974 (d, 1H, Hh). L = tpm: Yield: 81 mg (36.0%). Anal. Calcd for **3b^{red}·15H$_2$O·7CH$_3$OH**: C, 31.6; H, 6.1; N, 15.6. Found: C, 31.5; H, 5.0; N, 15.6. ^{1}H NMR (D_2O, 500 MHz), δ (ppm): 9.525 (s, H7), 8.537 (d, 2H, Ha), 8.404 (dd, 2H, Hd), 8.304 (d, 2H, H1), 8.135 (m, 3H, H3 + H4), 7.921 (dd, 2H, Hc), 7.377 (dd, 2H, Hb), 6.489 (d, 2H, H2), 6.308 (m, 2H, H5 + H6).

(TPP)[(L)(bpy)Ru(μ-NC)Cr(CN)$_5$] (L = tpy (4a) or tpm (4b)). The procedure is analogous to that of **3a** and **3b**, L = tpy: Yield: 102 mg (52.2%). Anal. Calcd for **4a·3H$_2$O**: C, 60.5; H, 4.2; N, 14.1. Found: C, 59.8; H, 3.8; N, 14.1. L = tpm: Yield: 83 mg (41.1%). Anal. Calcd for **4b·5H$_2$O**: C, 54.2; H, 4.4; N, 17.7. Found: C, 53.7; H, 4.2; N, 17.7.

Physical measurements

IR spectra were collected with a Nicolet FTIR 510P instrument, as KBr pellets. UV-visible spectra were recorded with a Hewlett-Packard 8453 diode array spectrometer in the range between 190 and 1100 nm. NMR spectra were measured in a Bruker ARX500 spectrometer, using deuterated solvents from Aldrich. Elemental analyses were performed with a Carlo Erba 1108 analyzer. Cyclic voltammetry measurements were performed under argon with millimolar solutions of the compounds, using a TEQ V3 potentiostat and a standard three electrode arrangement consisting of a glassy carbon disc (area = 9.4 mm^2) as the working electrode, a platinum wire as the counter electrode and a reference electrode. Depending on the situation the reference was a Ag/AgCl 3 M KCl standard electrode (for aqueous solutions) or a silver wire (non-aqueous solutions) plus an internal ferrocene (Fc) or decamethylferrocene ($Me_{10}Fc$) standard for organic solvents. KNO_3 1 M and tetra-*N*-butylammonium hexaflourophosphate ($TBAPF_6$) 0.1 M were used as supporting electrolytes in water and non-aqueous media respectively. All the potentials reported in this work are referenced to the standard Ag/AgCl saturated KCl electrode (0.197 V *vs.* NHE), the conversions being performed with literature values for the Fc^+/Fc or $Me_{10}Fc^+$/$Me_{10}Fc$ couples in different media.[13]

Excitation and emission spectra of the monomers were recorded in a PTI-Quantamaster spectrofluorometer, and in a PTI-QuantaMaster 50 in the case of **4a–b**. Quantum yields were measured in Argon-saturated solutions using $[Ru(bpy)_3]^{2+}$ (ϕ = 0.095[14] in ACN at 25 °C) and IR-140 (ϕ = 0.167[15] in EtOH at 25 °C, correcting by refractive index) as references. Time resolved luminescence measurements for the monomers were made using a PicoQuant FluoTime 100 Compact Fluorescence Lifetime Spectrometer, with a LDH-P-C-375 diode laser centered at 375 nm (300 ps FWHM) as the excitation source. Emission was filtered by a 620 nm cut-off filter. In the case of compounds **4a–b**, after exciting with a 400 nm centered laser (300 fs pulses generated by second-harmonic generation (SHG) of a regeneratively amplified mode-locked Ti:sapphire laser), emission was measured with a photomultiplier tube (Hammamatsu R928). Then the signal was collected and averaged on a Tektronix TDS3052 digitizing oscilloscope and transferred to a computer for kinetic analysis.

X-Ray structure determinations

Crystal structures of compounds **1–4a** and **1–3b** were determined with an Oxford Xcalibur, Eos, Gemini CCD area-detector diffractometer using graphite-monochromated Mo-Kα radiation (λ = 0.71069 Å) at 298 K. Data was corrected for absorption with CrysAlisPro, Oxford Diffraction Ltd, Version 1.171.33.66 analytically by face-indexing in the case of compounds **1a**, **1b**, **2b** and **3a** and applying an empirical absorption correction using spherical harmonics, implemented in SCALE3 ABSPACK scaling algorithm[16] in the case of compounds **2a**, **3b** and **4a**. The structures were solved by direct methods with SHELXS-97[17] and refined by full-matrix least-squares on F2 with SHELXL-97.[17] Hydrogen atoms were added geometrically and refined as riding atoms with a uniform value of Uiso. Only in compound **1a** structure, hydrogen atoms of solvent water molecule were located in the Fourier difference map and subsequently refined. In all other refined structures no other water hydrogen atoms were located in the difference map and hence were not included in the modeling. In structures **1a**, **1b** and **2a** some fluoride atoms of PF_6^- counterion were found disordered and refined as two split positions with 0.5 : 0.5 occupation ratios. In structures **1b**, **3a**, **4a** and **3b** one, two, two and five water solvent molecules, respectively, were found disordered and refined as two split positions with 0.5 : 0.5 occupation ratio. Crystals of compound **2a** were of poor quality and refined only up to R^1 = 0.12, however the structure is still useful for the overall discussion. Final crystallographic data and values of R^1 and wR are listed in Table S1 (see ESI†) while the main angles and distances are listed in Table 2 and S2 (see ESI†). CCDC 843186–84319 contains the supplementary crystallographic data for this paper (see ESI†).

Results

Synthesis

The synthesis of the complexes reported here is based on the well established anion substitution of the chloride precursors $[Ru(L)(bpy)Cl]^+$ in methanol or in water.[11,18–20] The TPP^+ salts of the $[M^{III}CN_6]^{3-}$ were chosen as precursors in order to obtain the salts of the corresponding dinuclear complexes with this cation, which can be crystallized from methanol–water mixtures.

Crystal structure determinations

The crystal structures of mononuclear complexes **1a–b** and **2a–b** and dinuclear complexes **3a–b** and **4a** were determined by X-ray

Published on 26 March 2012 on http://pubs.rsc.org | doi:10.1039/C2DT11869F
Downloaded by University of Michigan Library on 26 April 2012

Table 2 Selected bond distances and angles for the compounds **1a**, **1b**, **3a** and **3b**

1a	1b	3a	3b
		Distances (Å)	
Ru–CN	Ru–CN	$Ru–NC_{bridge}$	$Ru–NC_{bridge}$
1.995(3)	1.999(6)	2.062(5)	2.0346 (19)
RuC–N	RuC–N	$RuN–C_{bridge}$	$RuN–C_{bridge}$
1.145(4)	1.146(8)	1.149(8)	1.148 (3)
		$NC_{bridge}–Fe$	$NC_{bridge}–Fe$
		1.937(6)	1.949(2)
		Ru–Fe	Ru–Fe
		5.113	5.045
$Ru–N_{tpy}$	$Ru–N_{tpm}$	$Ru–N_{tpy}$	$Ru–N_{tpm}$
2.081 (3)	2.119 (4)	2.077 (5)	2.0608 (18)
2.064 (2)	2.090 (4)	2.071 (5)	2.0760 (18)
1.966 (2)	2.083 (4)	1.961 (5)	2.0902 (19)
		Angles (°)	
Ru–C–N	Ru–C–N	$Ru–N–C_{bridge}$	$Ru–N–C_{bridge}$
175.8(3)	175.0 (6)	168.5 (5)	163.58 (17)
		$N–C_{bridge}–Fe$	$N–C_{bridge}–Fe$
		176.9 (6)	172.89 (19)
$N_{tpy}–Ru–N_{tpy}$	$N_{tpm}–Ru–N_{tpm}$	$N_{tpy}–Ru–N_{tpy}$	$N_{tpm}–Ru–N_{tpm}$
79.47 (10)	85.72 (17)	80.1 (2)	86.76 (7)
79.10 (10)	85.46 (16)	79.1 (2)	86.15 (7)
	82.72 (17)		83.36 (7)
		Torsion	Torsion
		0.01	35.96

crystallography. Table 2 summarizes selected bond distances and angles and Fig. 1 shows the structures of the compounds **1a–b** and **3a–b** (see ESI† for **2a–b** and **4a**).

The differences in the coordination sphere of the mononuclear complexes are mainly related to the steric constraints of the tridentate ligands. The geometry of the terpyridine ligand imposes a short Ru–N distance for the central ring and a considerable departure of the 90° angle between the terminal and middle N atoms and the Ru expected for an octahedral environment. These differences are less pronounced in the trispirazolylmethane complexes as the geometry of this ligand imposes fewer restrictions on the position of the coordinated N atoms. Overall the Ru–N bonds are similar in all complexes reported here and in the range expected for Ru(II) polypyridines with little influence from the sixth ligand.

The structures of the dinuclear systems are somewhat different. While **3a** and **4a** show an almost linear arrangement of the metal center, and an eclipsed configuration of their equatorial ligands similar to structure observed in related complexes,[21] the structure of **3b** is less linear and presents a significant torsion angle of 36° around the cyanide bridge. This fact could be interpreted as evidence of stronger interaction between the metallic ions connected by the cyanide bridge in **3a** and **4a** compared to **3b**, although other parameters in the structure, namely the Ru–N_{bridge}, C–N_{bridge} and Fe–C_{bridge} distances, suggest that the interaction is similar and not particularly strong in the three systems. It is more likely that the differences arise from the intermolecular interactions observed in the crystal structure. The crystal structures of all the complexes containing terminal cyanides (**1a–b**, **3a–b**, **4a**) present hydrogen bonds from the N atom of the cyanide unit and crystallization water molecules. The other main interaction defining the structure of these salts is the π stacking between the polypyridine ligands in neighboring complexes (for example C···C bpy π stacking = 3.34 Å in **1b**).

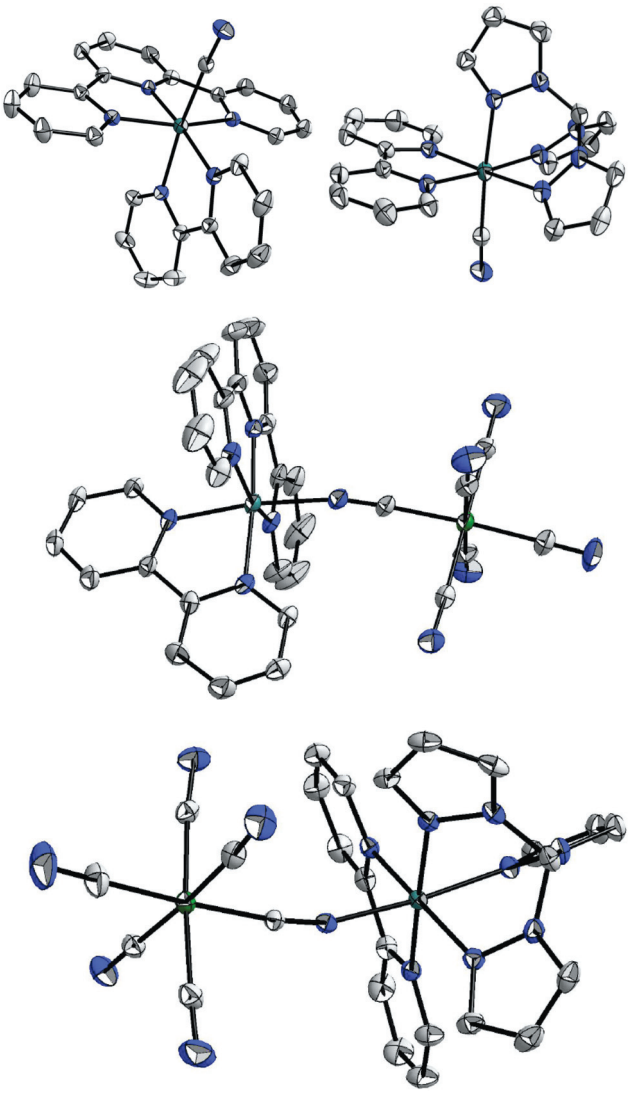

Fig. 1 Crystal structures of the complexes **1a** (top, left), **1b** (top, right), **3a** (middle) and **3b** (bottom). Ellipsoids drawn with 30% displacement probability. Hydrogen atoms, counterions and solvent molecules were omitted for clarity.

Electrochemistry

Cyclic voltammograms of the reported complexes are shown in Fig. 2, while the relevant electrochemical data is presented in Table 3.

The monomers **1a–b** and **2a–b** present one electron reversible oxidation and several quasi-reversible reductions (Fig. 2). The former corresponds to the $Ru^{II} \rightarrow Ru^{III}$ process and its potential depends mainly on the coordination sphere of ruthenium, being higher for the cyanide complexes **1a–b**. The complexes bearing a tpm ligand have a slightly lower Ru(III)–Ru(II) potential due to the higher basicity of this ligand, with this trend being observed for all the complexes reported here (Table 3). For the dinuclear complexes **3a–b** and **4a–b** the $Ru^{II} \rightarrow Ru^{III}$ wave shows an adsorption process due to the neutral charge of the oxidized

 This journal is © The Royal Society of Chemistry 2012

Downloaded by University of Michigan Library on 26 April 2012
Published on 26 March 2012 on http://pubs.rsc.org | doi:10.1039/C2DT11869F

Table 3 Redox potentials for the Ru(III)/Ru(II), M(III)/M(II) and L/L$^-$ couples of the complexes **1–4** in different solvents

Complex	Solvent	$E_{1/2}$(Ru)/V (ΔE_p/mV)	$E_{1/2}$(M)/V (ΔE_p/mV)	$E_{1/2}$(L)/V (ΔE_p/mV)
1a	Acetonitrile	1.18 (130)	—	−1.30 (190)
1b	Acetonitrile	1.14 (100)	—	−1.39 (100)
2a	Acetonitrile	1.04 (90)	—	−1.25 (100)
2b	Acetonitrile	0.96 (100)	—	−1.42 (110)
3a	Water	0.88 (80)	0.18 (80)	na
	Acetonitrile	1.02 (100)	−0.64 (80)	−1.39 (80)
3b	Water	0.85 (90)	0.21 (100)	na
	Acetonitrile	0.93 (180)	−0.65 (180)	−1.57 (120)
4a	Acetonitrile	1.10 (190)	−1.83[a]	−1.28 (120)
4b	Acetonitrile	1.00 (180)	−1.73[a]	−1.41 (110)

[a] Irreversible wave, cathodic peak.

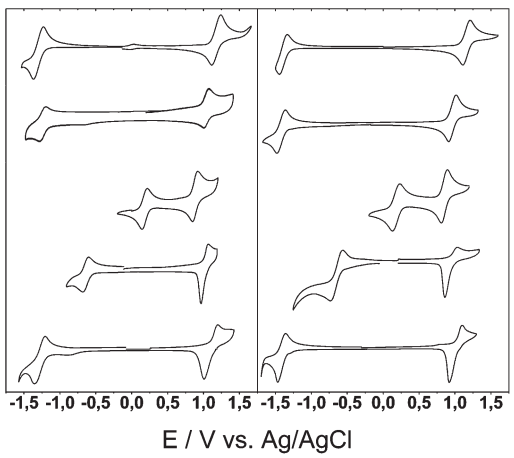

Fig. 2 Cyclic voltammograms in acetonitrile of the complexes **1a**, **2a**, **3a** (water), **3a** (acetonitrile), **4a** (left panel, from top to bottom), and **1b**, **2b**, **3b** (water), **3b** (acetonitrile), **4b** (right panel, from top to bottom).

species. The reduction waves are centered in the polypyridinic ligands and they are slightly higher for the process centered in the tpy ligand.

For the dinuclear compounds **3a–b** a reduction wave is observed between the oxidation wave for $Ru^{II} \rightarrow Ru^{III}$ process and the reduction of the polypyridine ligands. Its potential is highly solvent sensitive (Table 3, Fig. 2) which is a distinctive feature of the cyanocomplexes, and thus we assign it to the $Fe^{III} \rightarrow Fe^{II}$ process. In these systems the reduction of the polypyridine ligand is shifted to lower potentials due to the effect of the additional negative charge associated with the additional reduction in these iron dinuclear compounds (Fig. 3).

For the dinuclear compound **4a** two quasi-reversible waves for the reduction of the polypyridne ligand are followed by an irreversible process, which is absent in the dinuclear complex **3a** (Fig. 3). We assign it as the $Cr^{III} \rightarrow Cr^{II}$ reduction which is irreversible due to the ligand loss on the Cr(II) moiety.

Electronic spectroscopy

Fig. 4 shows the observed absorption spectra for all the complexes reported in this work, with the absorption maxima information listed in Table 4. All the explored complexes exhibit the

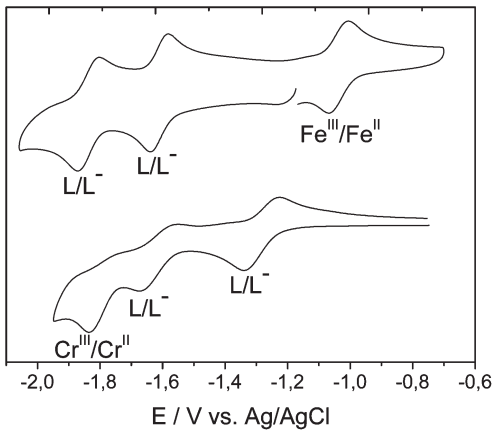

Fig. 3 Cyclic voltammogram at cathodic potentials of the complexes **3a** (top) and **4a** (bottom) in acetonitrile.

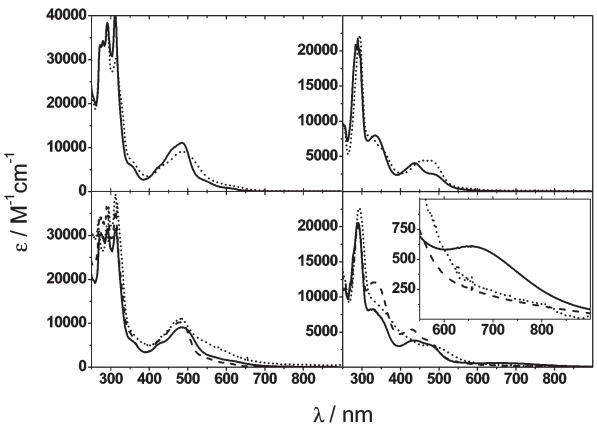

Fig. 4 UV-vis-NIR absorption in acetonitrile of complexes **1a** (solid line), **2a** (dashed line) (left panel, top), **1b** (solid line), **2b** (dashed line) (right panel, top), **3a** (solid line), **3a^{red}** (dotted line), **4a** (dashed line) (left panel, bottom), **3b** (solid line), **3b^{red}** (dotted line), **4b** (dashed line) (right panel, bottom).

electronic spectroscopic features expected from ruthenium polypyridine chromophores; sharp ligand centered $\pi \rightarrow \pi^*$ transitions in the UV and intense broad bands in the visible region, corresponding to $Ru^{II} \rightarrow \pi^*$ (polypyridine ligand) MLCT transition (Fig. 4 and Table 4).

For complexes bearing the tpy ligand (Fig. 4, left panel), only one of the two expected MLCT bands is observed, with the $\pi \rightarrow \pi^*$ band of tpy at 310 nm obscuring the high energy MLCT. The two components are clearly visible for the complexes with the tpm ligand, each being a superposition of a MLCT to each of the two polydentate ligands. Compound **3b** in acetonitrile present an additional band at 653 nm which corresponds to the $Ru^{II} \rightarrow Fe^{III}$ MM′CT transition. This transition in not visible for **3a** in acetonitrile, probably because it is buried under the MLCT band, but becomes visible in other solvents (Table 5, Fig. 5).

The energy of this MM′CT band in different solvents correlates well (see ESI†) with the difference in the redox potential (Table 3) between the iron and ruthenium centers, confirming its nature. Also the transition moment (see ESI†) of the MM′CT band in different solvents correlates with the energy of the

Published on 26 March 2012 on http://pubs.rsc.org | doi:10.1039/C2DT11869F
Downloaded by University of Michigan Library on 26 April 2012

Table 4 UV-vis absorption properties for the complexes reported in acetonitrile

Complex	$\pi \rightarrow \pi^*$ λ/nm (ε M^{-1} cm^{-1})	MLCT λ/nm (ε M^{-1} cm^{-1})
1a	272 (33400)	
	279 (34260)	354 (5950) (sh)
	311 (40330)	485 (11080)
2a	272 (33400)	
	279 (34260)	357 (6820) (sh)
	313 (30430)	487 (9080)
3a^{red}	275 (36390)	
	281 (36390)	nd
	312 (39290)	479 (10550)
3a	271 (30080)	
	291 (31240)	361 (5600) (sh)
	313 (31330)	484 (9090)
4a	272 (34700)	
	290 (36370)	353 (7610) (sh)
	312 (35650)	478 (10200)
1b	287 (21440)	333 (8100)
		436 (4070)
2b	293 (22370)	322 (7910)(sh)
		458 (4410)
3b^{red}	293 (22660)	355 (8260)(sh)
		416 (4250)(sh)
3b	290 (20540)	329 (8240)
		436 (3790)
4b	290 (20070)	332 (12100)
		430 (5340)

Table 5 MM′CT transition energies and metal–metal coupling for the mixed-valence species **3a** and **3b**

	MM′CT $\nu/10^3$ cm^{-1} ($\varepsilon/10^3$ M^{-1} cm^{-1})		H_{12}/cm^{-1}		μ^2/(eÅ)^2	
Solvent	**3a**	**3b**	**3a**	**3b**	**3a**	**3b**
ACN	nd	15.3 (607)	nd	nd	nd	nd
EtOH	14.1 (669)	12.6 (705)	nd	757	nd	1.07
MeOH	13.2 (1116)	12.2 (842)	973	814	1.37	1.17
Water	9.7 (2092)	8.7 (1887)	1303	1213	4.04	3.02

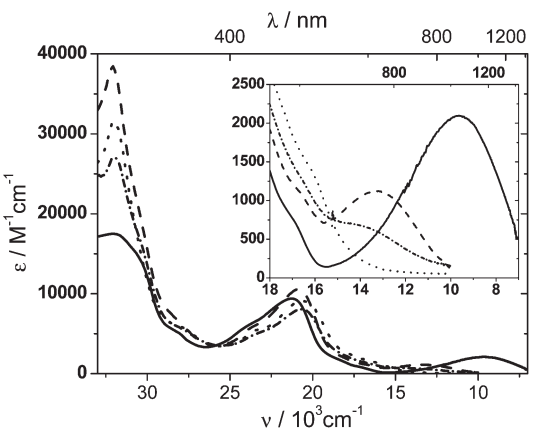

Fig. 5 UV-vis-NIR absorption of the complex **3a** in water (solid line), methanol (dashed line), ethanol (dashed-dotted line), acetonitrile (dotted line). Inset: MM′CT bands.

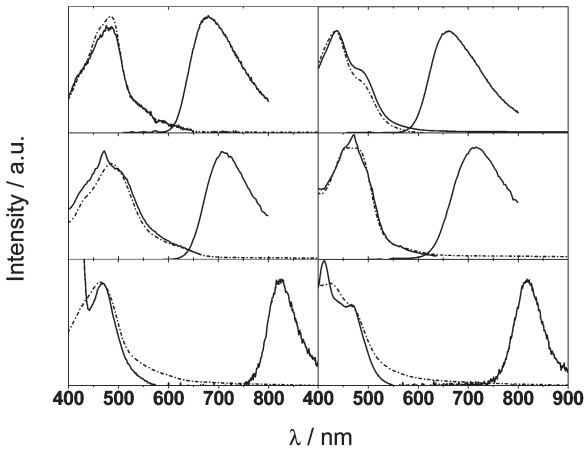

Fig. 6 Excitation (solid line), absorption (dotted line) and emission (solid line) in acetonitrile at 25 °C of the complexes **1a**, **2a**, **4a** (left panel from top to bottom) and **1b**, **2b**, **4b** (right panel from top to bottom).

Table 6 Emission properties for the reported complexes in acetonitrile at 25 °C

Complex	λ_{em}/nm	$\phi_{em} \times 10^3$	τ/ns
1a	679	0.12	5.9
2a	709	0.13	10.4
3a^{red}	—	<0.01	—
3a	—	<0.01	—
4a	822	2.6	2.80×10^5
1b	662	0.95	43.6
2b	715	0.23	20.1
3b^{red}	—	<0.01	—
3b	—	<0.01	—
4b	818	2.6	3.28×10^5

transition, a feature previously observed for other mixed valence systems with a Fe(III) hexacyanide moiety.[21] Application of the Mulliken–Hush expression results in values for H_{12} (the coupling between the metal centers, Table 5) similar to the ones calculated for other cyanide-bridged dinuclear systems[3,22–25] and suggests small but significant mixing between the d orbitals of the metallic ions.

We do not observe the MM′CT band for complexes **4a–b**. This band is expected to be at higher energy than the lower MLCT according to the position of the irreversible reduction of the Cr(III) moiety with respect to the reduction of the polypyridines (Table 3), suggesting that it might be buried under the MLCT and can not be distinguished, as it is expected to be broad and not very intense.

Photophysical properties

The four mononuclear complexes reported in this work luminesce at room temperature in acetonitrile (Fig. 6), with the relevant data listed in Table 6. Solutions are photostable with no significant ligand loss observed after the excitation. The observed broad emission is shifted to the red upon replacement of the cyanide ligand (**1a–b**) by thiocyanate (**2a–b**). This bathochromic shift with the exchange of non-chromophoric ligands is

This journal is © The Royal Society of Chemistry 2012

Published on 26 March 2012 on http://pubs.rsc.org | doi:10.1039/C2DT11869F
Downloaded by University of Michigan Library on 26 April 2012

consistent with the effect observed in redox potentials for the Ru(III)/Ru(II) couple (Table 3), and confirms the MLCT state origin of this emission. Replacement of tpy by tpm has very little influence on the energy maxima of the emission band. The main effect is longer life times and higher emission quantum yields for the tpm complexes, although the four reported monomers are weak emitters.

The lifetimes and emission quantum yields for these complexes are consistent with the reported properties of other tpy[11,18,20,26–29] and tpm[19,30] complexes. This photophysical response has been ascribed to the presence of a short-lived metal-centered (MC) state of low energy. DFT calculations[31] in tpy complexes has confirmed this low energy state which is due to the constraints in the coordination sphere of the Ru caused by the geometry of the polydentate ligands.[28]

Unlike some other complexes in this family,[27,30,32] **1a–b** and **2a–b** show no evidence of ligand loss upon absorption in the MLCT bands. For example, $[Ru(tpy)(bpy)Cl]^+$ shows prominent ligand loss upon absorption in the same region of the spectrum, thus we conclude that in the cases reported here the Ru–X bond should be stronger than the Ru–Cl bond with some π back bonding contribution.

The photophysical properties of dinuclear complexes are very different from those of the monomers. Both chromium dinuclear complexes, **4a–b**, show a narrow NIR emission at room temperature in acetonitrile (Table 6, Fig. 6). The excitation spectra of these compounds measured at the emission maxima follow very closely their absorption spectra in the visible (Fig. 6), which is mainly due to the transitions in the Ru(L)(bpy) fragment. The wavelength of emission (~820 nm), its band shape and its very long lifetime indicate very clearly that this emission has its origin in a metal centered (MC) excited state from the $[Cr(CN)_6]^{3-}$.[33]

This evidence suggests that the absorption is initiated in the ruthenium chromophore leading probably to the population of the ^{3}MLCT excited state as observed for the monomers. This is followed by an energy transfer from the ^{3}MLCT excited state to a MC excited state in the chromium moiety. The process is very efficient, with quantum yields of emission for complexes **4a–b** similar to the quantum yields reported for the $[Cr(CN)_6]^{3-}$ monomer and for the dinuclear complex reported by Bignozzi *et al.*[33] This high yield suggests that the efficiency of population of the chromium MC excited state at the expense of Ru MLCT excited state is essentially unitary for complexes **4a–b**. This high efficiency for the energy transfer process from weak emitters with short lifetimes, like the fragments Ru(tpy)(bpy) and Ru(tpm)(bpy), implies fast transfer rates, probably in the ps time scale. As the process involves excited states of different multiplicity (a ^{3}MLCT state and a ^{2}MC state), the Forster mechanism is ruled out.[33]

In contrast with the chromium complexes, iron dinuclear complexes do not show any significant emission. This lack of response could also be due to the coupling between the excited states mediated by the cyanide bridge. In complexes **3a–b^{red}**, the energy transfer to the low energy MC states in the iron(II), which are expected to be at ~800 nm by analogy with **4a–b**, should result in thermal deactivation. For the oxidized form of these complexes there is also another mechanism available. The MM′ CT states are closer in energy to the MLCT Ru-centered states (bands overlapping in the UV-vis spectra in ACN, Fig. 4) than the MC states (~800 nm). Thus, after excitation an electron transfer to the Fe(III) could occur, effectively quenching the emission of the ruthenium moiety.[34] Transient absorption measurements are underway to explore the nature of this processes.

Conclusions

The structural and spectroscopic properties of the mononuclear complexes described in this work fit very well with the reported properties of other [Ru(tpy)(bpy)X] and [Ru(tpm)(bpy)X] complexes, but unlike the other reported systems the complexes **1a–b** and **2a–b** show no evidence of ligand loss probably due to a combination of a stronger Ru–X bond and a shift to lower energies of the ^{3}MLCT excited state.

The properties of the MM′CT band observed in the mixed valence dinuclear complexes **3a–b** points to a significant coupling between the metallic centers. The M–M′ coupling results in complete quenching of the Ru centered ^{3}MLCT excited state through efficient electron transfer to a MM′CT state (**3a–b**) or energy transfer to an iron centered d–d state (**3a–b^{red}**) that decay without emission. For the chromium dinuclear complexes **4a–b** instead, the coupling between the excited states mediated by the cyanide bridge results in an energy transfer to the chromium-centered excited state, clearly revealed by its emission.

Our results show that the energy transfer across the cyanide bridge is highly efficient as even weak emitters with relatively short lived excited states are able to undergo energy transfer. This outcome suggests that polynuclear cyanide bridged arrays can be viable systems for the construction of multichromophoric antenna units. The observed rapid energy transfer offers the possibility of incorporating different chromophores, even weak emitters, and thus a large variety of molecules can be used to tune the array. The constraint to be considered in the design of the antenna should be the avoidance of fragments with low energy MC states or MM′CT states which may be thermally deactivated (like the iron complexes reported here). One clear way to avoid this limitation is to use second and third row transition metals that have MC states of higher energy. Coordination of a ruthenium polypyridine chromophore to $[Ru(CN)_6]^{4-}$ or $[Os(CN)_6]^{4-}$ anions is already under way in our labs.

Acknowledgements

The authors thank the University of Buenos Aires and the Consejo Nacional de Investigaciones Científicas y Técnicas (CONICET) for funding, and Prof. P. F. Aramendía for kind help with the lifetime measurements. LBV and PA are members of the scientific staff of CONICET. This material is based upon work supported by the National Science Foundation under CHE – 1058638. AC also acknowledges technical support by ALN.

Notes and references

1 L. Catala, D. Brinzei, Y. Prado, A. Gloter, O. Stephan, G. Rogez and T. Mallah, *Angew. Chem., Int. Ed.*, 2009, **48**, 183–187.
2 J. T. Culp, J. H. Park, F. Frye, Y. D. Huh, M. W. Meisel and D. R. Talham, *Coord. Chem. Rev.*, 2005, **249**, 2642–2648.

View Online

3 F. Scandola, R. Argazzi, C. A. Bignozzi, C. Chiorboli, M. T. Indelli and M. A. Rampi, *Coord. Chem. Rev.*, 1993, **125**, 283–292.
4 D. L. Reger, T. C. Grattan, K. J. Brown, C. A. Little, J. J. S. Lamba, A. L. Rheingold and R. D. Sommer, *J. Organomet. Chem.*, 2000, **607**, 120–128.
5 A. Llobet, P. Doppelt and T. J. Meyer, *Inorg. Chem.*, 1988, **27**, 514–520.
6 B. P. Sullivan, J. M. Calvert and T. J. Meyer, *Inorg. Chem.*, 1980, **19**, 1404–1407.
7 K. J. Takeuchi, M. S. Thompson, D. W. Pipes and T. J. Meyer, *Inorg. Chem.*, 1984, **23**, 1845–1851.
8 P. Albores, L. D. Slep, T. Weyhermuller, E. Rentschler and L. M. Baraldo, *Dalton Trans.*, 2006, 948–954.
9 P. A. W. Dean, K. Fisher, D. Craig, M. Jennings, O. Ohene-Fianko, M. Scudder, G. Willett and I. Dance, *Dalton Trans.*, 2003, 1520–1528.
10 W. L. F. Armarego and D. D. Perrin, *Purification of Laboratory Chemicals*, Oxford, UK, 1996.
11 P. Belser, A. Vonzelewsky, A. Juris, F. Barigelletti and V. Balzani, *Gazz. Chim. Ital.*, 1985, **115**, 723–729.
12 W. K. Seok, S. W. Moon and M. Y. Kim, *Bull. Korean Chem. Soc.*, 1998, **19**, 1207–1210.
13 I. Noviandri, K. N. Brown, D. S. Fleming, P. T. Gulyas, P. A. Lay, A. F. Masters and L. Phillips, *J. Phys. Chem. B*, 1999, **103**, 6713–6722.
14 Y. Yamamoto, Y. Tamaki, T. Yui, K. Koike and O. Ishitani, *J. Am. Chem. Soc.*, 2010, **132**, 11743–11752.
15 K. Rurack and M. Spieles, *Anal. Chem.*, 2011, **83**, 1232–1242.
16 SCALE3 ABSPACK: Empirical absorption correction – CrysAlis – Software package, Oxford Diffraction Ltd., Oxford, 2006.
17 G. M. Sheldrick, *SHELXS97 and SHELXL97, Programs for Crystal Structure Resolution*, University of Göttingen, Göttingen, Germany, 1997.
18 A. Ponce, M. Bachrach, P. J. Farmer and J. R. Winkler, *Inorg. Chim. Acta*, 1996, **243**, 135–140.
19 N. E. Katz, F. Fagalde, N. D. L. de Katz, M. G. Mellace, I. Romero, A. Llobet and J. Benet-Buchholz, *Eur. J. Inorg. Chem.*, 2005, 3019–3023.
20 S. C. Rasmussen, S. E. Ronco, D. A. Mlsna, M. A. Billadeau, W. T. Pennington, J. W. Kolis and J. D. Petersen, *Inorg. Chem.*, 1995, **34**, 821–829.
21 P. Albores, L. D. Slep, T. Weyhermuller and L. M. Baraldo, *Inorg. Chem.*, 2004, **43**, 6762–6773.
22 A. V. Macatangay and J. F. Endicott, *Inorg. Chem.*, 2000, **39**, 437–446.
23 F. W. Vance, R. V. Slone, C. L. Stern and J. T. Hupp, *Chem. Phys.*, 2000, **253**, 313–322.
24 M. A. Watzky, A. V. Macatangay, R. A. VanCamp, S. E. Mazzetto, X. Q. Song, J. F. Endicott and T. Buranda, *J. Phys. Chem. A*, 1997, **101**, 8441–8459.
25 L. M. Baraldo, P. Forlano, A. R. Parise, L. D. Slep and J. A. Olabe, *Coord. Chem. Rev.*, 2001, **219**, 881–921.
26 C. Y. Wong, M. C. W. Chan, N. Y. Zhu and C. M. Che, *Organometallics*, 2004, **23**, 2263–2272.
27 I. M. Dixon, E. Lebon, G. Loustau, P. Sutra, L. Vendier, A. Igau and A. Juris, *Dalton Trans.*, 2008, 5627–5635.
28 R. M. Berger and D. R. McMillin, *Inorg. Chem.*, 1988, **27**, 4245–4249.
29 J. D. Petersen, L. W. Morgan, I. Hsu, M. A. Billadeau and S. E. Ronco, *Coord. Chem. Rev.*, 1991, **111**, 319–324.
30 K. R. Barqawi, A. Llobet and T. J. Meyer, *J. Am. Chem. Soc.*, 1988, **110**, 7751–7759.
31 E. Jakubikova, W. Chen, D. M. Dattelbaum, F. N. Rein, R. C. Rocha, R. L. Martin and E. R. Batista, *Inorg. Chem.*, 2009, **48**, 10720–10725.
32 C. R. Hecker, P. E. Fanwick and D. R. McMillin, *Inorg. Chem.*, 1991, **30**, 659–666.
33 C. A. Bignozzi, M. T. Indelli and F. Scandola, *J. Am. Chem. Soc.*, 1989, **111**, 5192–5198.
34 It is worth to notice that compounds **4a–b** are unlikely to undergo this last mechanism because, as can be inferred from the reduction potentials (Table 3), their MM′CT states (reducing the Cr(III) moiety) are higher in energy than MLCT states (reducing the polypyridine ligands).

Downloaded by University of Michigan Library on 26 April 2012
Published on 26 March 2012 on http://pubs.rsc.org | doi:10.1039/C2DT11869F

 This journal is © The Royal Society of Chemistry 2012